

Recent progress in perpendicularly magnetized Mn-based binary alloy films

Zhu Li-Jun, Nie Shuai-Hua, and Zhao Jian-Hua[†]

State Key Laboratory of Superlattices and Microstructures, Institute of Semiconductors, Chinese Academy of Sciences, P. O. Box 912, Beijing 100083, China

In this article, we review the recent progress in growth, structural characterization, magnetic properties and related spintronic devices of tetragonal Mn_xGa and Mn_xAl thin films with perpendicular magnetic anisotropy. In the first part of this review, we present a brief introduction to the demands for perpendicularly magnetized materials in spintronics, magnetic recording and permanent magnets applications, and the most promising candidates of tetragonal Mn_xGa and Mn_xAl with strong perpendicular anisotropy. Then, in the second and third parts, we focus on the recent progress of perpendicularly magnetized Mn_xGa and Mn_xAl , respectively, including their lattice structures, bulk synthesis, epitaxial growth, structural characterizations, magnetic and other spin-dependent properties, and spintronic devices like magnetic tunneling junctions, spin valves and spin injector into semiconductors. Finally, we give a summary and a perspective of these perpendicularly magnetized Mn-based binary alloy films for future applications.

Keywords: Spintronics, Magnetic material, Perpendicular magnetic anisotropy, Semiconductors
PACS: 85.70.2w, 81.05.-t, 75.30.Gw, 85.30.2z

1. Introduction

Ferromagnetic films with high perpendicular magnetic anisotropy (K_u) have attracted much attention for their potential applications in nanoscale magnetic devices with high thermal stability.^[1-4] Spin valves and magnetic tunneling junctions (MTJs) with high K_u have been demonstrated to allow for realization of high-sensitivity magnetoresistive sensors, spin-transfer-torque (STT) switching Gbit-class magnetoresistive random access memory (MRAM) and high-power oscillators.^[2-5] Magnetic materials which have high K_u along with high spin polarization (P), high Curie temperature (T_c), flexible magnetization (M_s) and low magnetic damping constant (α) are the most ideal combination for spin-transfer-torque applications to facilitate reliable switching under the current density below 10^5 A/cm².^[2-4] Moreover, ferromagnetic films with both high K_u and good compatibility with semiconductor allow for not only the development of ferromagnetic

metal/semiconductor hybrid devices including spin field effect transistor,^[6,7] spin Hall transistor,^[8] light emitting diodes^[9,10] and lateral spin valves^[12] with perpendicular anisotropy, but also high-density integration of metallic spintronics functional devices like nonvolatile magneto-resistive random access memory on semiconductor photonic and electronic circuits.^[12,13-17] These approaches could also perform logic, communications and storage within the same materials technology taking advantage of nonvolatility, increased integration density, increased speed and decreased energy consumption compared with conventional charge-based devices.^[18] Furthermore, demand for increasing high-density data storage leads to the replacement of in-plane magnetic recording by perpendicular magnetic recording. Perpendicular magnetic recording with areal density beyond 10 Tb/inch² requires films with high K_u up to 10^7 erg/cc and moderate magnetization M_s .^[19] Too high M_s may result in strong coupling between adjacent bits, while too low M_s brings about low signal-noise ratio. Besides, rare-earth magnets provide the backbone of many products including computers, mobile phones, electric cars and wind-power generators. However, because of both the increasing limited availability and high costs of mining and processing of rare-earth elements, new kind of rare-earth-free magnets are urgently needed.^[16, 20] Permanent magnets applications require materials that have large magnetic energy product, high intrinsic and extrinsic coercivities and linear demagnetization curve in the second quadruple.

As the most outstanding representatives, perpendicularly magnetized Mn-binary alloys Mn_xGa ($MnGa$) and Mn_xAl ($MnAl$) have attracted much attention and have been studied intensively in the past couple of decades. $L1_0$ - $MnGa$ ($D0_{22}$ - Mn_3Ga) alloys are theoretically expected to have K_u of 26 (20) Merg/cc,^[21,22] M_s of 845 (305) emu/cc,^[16,21-23] $(BH)_{max}=(2\pi M_s)^2$ of 28 (3.7) MGOe,^[17,24] P of 71% (88%) at the Fermi level^[17,21,24,25] and α of 0.0003 (0.001),^[22] respectively. Moreover, $L1_0$ - $MnAl$ are theoretically predicted to have a K_u of 15 Merg/cc, M_s of 800 emu/cc (or 2.37 μ_B /Mn) and $(BH)_{max}=(2\pi M_s)^2$ of 12.64 MGOe.^[26,27] These fascinating magnetic properties make $MnGa$ and $MnAl$ promising in spintronics, ultrahigh-density magnetic recording and economical permanent magnets applications. Moreover, many experimental attempts have been made to the preparation and characterization of $MnGa$ and $MnAl$ bulks and films, and their related spintronic devices like magnetic tunneling junctions, spin valve and spin-injection devices. In this article, we will present an overview of recent progress on the growth, structural characterization, magnetic properties and some other properties of perpendicularly magnetized Mn_xGa and Mn_xAl alloys and their related spintronic devices.

* Project supported by NSFC 11127406

[†] Corresponding author: jhzhao@red.semi.ac.cn

2. Mn_xGa with perpendicular magnetic anisotropy

2.1 Lattice structure and synthesis of Mn_xGa bulks

Alloys of Manganese (Mn) and Gallium (Ga) have quite complicated phase diagram (Fig. 1a) with several magnetically ordered phases.^[28-30] This review is mainly confined to two most interesting tetragonal phases with strong magnetism and high Curie temperature: the first is $L1_0$ -ordered (γ_3) thermal-dynamically ferromagnetic phase for $0.76 \leq x \leq 1.8$,^[17,31,32] the second is $D0_{22}$ -ordered (ϵ) ferrimagnetic phase, forming when $2 \leq x < 3$.^[25,33-36] The lattice units of both $L1_0$ -MnGa and $D0_{22}$ -Mn₃Ga are outlined in Fig. 1(b). The lattice unit of $L1_0$ -MnGa consists of Mn and Ga monatomic layers stacked alternately along the c axis. The lattice constants of $L1_0$ -MnGa bulk (space group $P4/mmm$) are $a=3.88$ - 3.90 Å and $c=3.64$ - 3.69 Å.^[31,32] Bither *et al.* synthesized $L1_0$ -Mn_xGa ($1.2 < x \leq 1.5$) polycrystalline bulks.^[31] Lu *et al.* systemically investigated the crystalline structures of Mn_xGa bulks in a broad composition range of $1.15 < x < 1.89$.^[32] For perfect stoichiometric $L1_0$ -MnGa ($x=1$), each Mn atom is expected to contribute a magnetic moment of $2.51 \mu_B$ (corresponding to magnetization of 845 emu/cc); the magnetism of $L1_0$ -Mn_xGa may also strongly be influenced by compositions and strains.^[16,17,23,25,31,36] As theoretically predicted, excess Mn atoms will align antiparallel to the rest and result in compensation, and strains will also induce a decrease of Mn moment.^[23,31] For $D0_{22}$ -Mn_xGa bulk (space group $I4/mmm$), the lattice constants are $a=3.90$ - 3.94 Å and $c=7.10$ - 7.17 Å.^[33-35] Krén and Kádár obtained $D0_{22}$ -Mn_{2.5}Ga bulks by annealing hexagonal

$D0_{19}$ -Mn_xGa at 350-400 °C for 1-2 weeks, and revealed the ferrimagnetism with Mn atom magnetic moment of $2.8 \pm 0.3 \mu_B$ and $1.6 \pm 0.2 \mu_B$ at site I and site II, respectively, by neutron diffraction measurement.^[33] Niida *et al.* and Winterlik *et al.* synthesized polycrystalline $D0_{22}$ -Mn_xGa bulks in the composition range of $1.94 \leq x \leq 2.85$ ^[34] and $2 \leq x \leq 3$,^[25] respectively, and revealed the composition-sensitive magnetization in the magnetically frustrated ferrimagnets. With Mn content increasing, lattice constant a slightly increases or keeps constant, while c always decreases monotonically.^[25, 31-36] Huh *et al.* synthesized Mn_xGa nano-ribbons with $L1_0$ ($x=1.2, 1.4, 1.6$) and $D0_{22}$ -ordering ($x=1.9$) using arc-melting and melt-spinning followed by a heat treatment and investigated their magnetic and transport behaviors.^[37] The Curie temperature of Mn_xGa nano-ribbons are found to increase with increasing x . All the ribbons are metallic transport behavior, in consistent with MnGa films.

The magnetic properties of Mn_xGa alloys, especially giant perpendicular anisotropy, high spin polarization, high Curie temperature, flexible magnetization and low magnetic damping constant are promising for applications of magnetic recording, permanent magnets and spintronics like magnetic sensors, memories and logics.^[16,17] Reliable growth of smooth MnGa thin films and effective tailoring of the magnetism are of particular importance for the possible practical applications in not only metal spintronics but also semiconductor spintronics. In the following, we will overview the recent progress in the growth and characterizations of $L1_0$ -MnGa films.

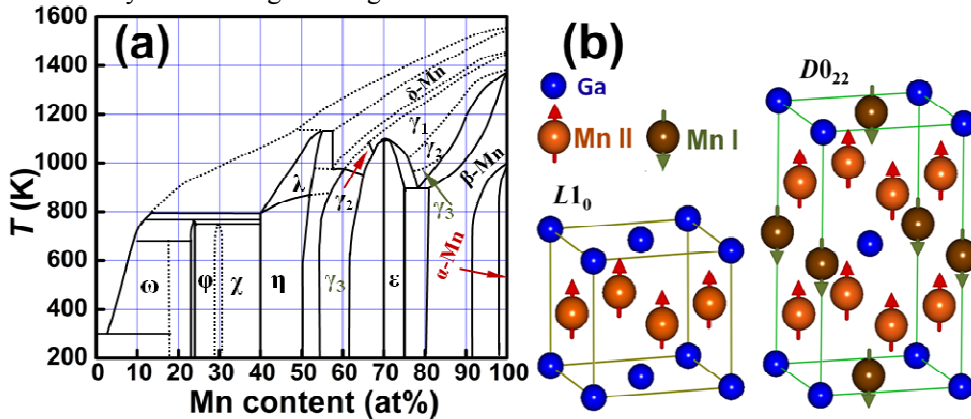


Fig. 1. (a) Phase diagram of Mn-Ga alloys, based on [30]; (b) Lattice unit of MnGa with $L1_0$ (left) and $D0_{22}$ (right), arrows stand for magnetic moment directions of Mn atoms (Reprinted with permission from [17]).

2.2 Growth and magnetic properties of Mn_xGa epitaxial films

In recent couple of decades, a great deal of effort has been made on growth of $L1_0$ and $D0_{22}$ -Mn_xGa films by magnetron sputtering or molecular-beam epitaxy (MBE). Since Krishnan and Tanaka *et al.* respectively observed square perpendicular hysteresis of Mn_xGa ($1.2 < x < 1.5$) grown on GaAs (001) by magneto-optical, magnetic and

transportation measurements in the early years of 1990s,^[38,39] the growth and characterizations of $L1_0$ -Mn_xGa films have been intensively studied on many kinds of substrates, such as GaN, GaSb, Si, Al₂O₃ and MgO with different buffer layers (ScN and Cr).^[36, 40-44] However, only a few of those films on GaAs and MgO demonstrated magnetic perpendicular anisotropy. $D0_{22}$ -Mn_xGa films have been prepared mainly on MgO (001)

substrates.^[22,35,36,45-47] Wu *et al.* reported magnetic and magneto-transport properties of Mn_xGa ($x=2.5$ and 2.0) epitaxial films on Cr-MgO (001) and even found perpendicular anisotropy in 5 nm-thick films.^[45,47] Kurt *et al.* prepared stoichiometric $D0_{22}$ - Mn_3Ga films with perpendicular easy axis on MgO, Pt-MgO and Cr-MgO, and observed the spin polarization of 58% (40%) in Mn_3Ga (Mn_2Ga).^[35,47] Recently, Nummy *et al.* and Zha *et al.* reported nanostructured Mn_xGa films on Si/SiO₂ with coercivity over 20 kOe and discussed the possibility for permanent magnet applications, respectively.^[48,49] Motivated by the great application potential and inspiring result of Mn_xGa alloys, we prepared Mn_xGa epitaxial films in a wide composition range ($0.76 \leq x \leq 2.60$) on GaAs (001) substrates by MBE, and carried out detailed studies on the tailoring of magnetism in these films with giant perpendicular anisotropy, ultrahigh coercivity and large energy product.^[16,17]

Table 1. Lattice constants of representative metals, insulators and semiconductors and calculated misfit in respect to $D0_{22}$ - Mn_3Ga ($a=3.910$ Å), $L1_0$ - $MnGa$ ($a=3.886$ Å) and $L1_0$ - $MnAl$ ($a=3.920$ Å). * represents the lattice constants after 45° in-plane rotation ($a^*=a/\sqrt{2}$).

buffer	a (Å)	$f_{D0_{22}-Mn_3Ga}$ (%)	f_{L1_0-MnGa} (%)	f_{L1_0-MnAl} (%)
Cu	3.61	8.3	7.6	8.6
Pd	3.89	0.5	-0.1	0.8
Pt	3.92	-0.3	-0.9	0
Au	4.08	-4.2	-4.8	-3.9
Ag	4.09	-4.4	-5.0	-4.2
Al	4.05	-3.5	-4.0	-3.2
Cr	4.07*	-4.0	-4.6	-3.8
Si	3.94*	-0.8	-1.4	-0.5
SrTiO ₃	3.91	0	0.8	0.3
GaAs	4.00*	-2.1	-2.7	-1.9
MgO	4.21	-7.2	-7.8	-7.0
InAs	4.28*	-8.6	-9.1	-8.4
AlAs	4.00*	-2.2	-2.7	-1.9

To realize the practical applications, especially for spintronics, it is essential to choose suitable substrates with small lattice misfit for epitaxial growth of Mn_xGa films simultaneously with high magnetic performance, good structural quality and smooth surface. Table 1 summarizes the in-plane lattice constants of representative metals, insulators and semiconductors with (001) orientation and calculated misfit f of $D0_{22}$ - Mn_3Ga ($a=3.910$ Å) and $L1_0$ - $MnGa$ ($a=3.886$ Å). Simply in view of lattice misfit, Pt (001), Pd (001), Si (001), SrTiO₃ (001) and GaAs (001) should be the best choices for epitaxial growth of both $D0_{22}$ and $L1_0$ films. To our best knowledge, the report of both $L1_0$ - and $D0_{22}$ - Mn_xGa

epitaxial films grown on Pd is still lacking. Perpendicularly magnetized $L1_0$ - Mn_xGa was not available on Si (001) probably due to strong reaction between metal layer and active silicon though f between $L1_0$ - $MnGa$ and Si (001) is only 1.4%.^[43] So far, only Pt, GaAs and SrTiO₃ buffers have been experimentally confirmed to be good choice for epitaxial growth of Mn_xGa films with flat surface and high crystalline quality.^[16, 17, 35, 47] As a recent review outlined,^[24] the surfaces of Mn_xGa films on Cr and MgO buffers appeared to be very rough with discontinuous islands,^[47] whereas films on Pt and GaAs buffers exhibited very smooth surfaces, since the misfit of $D0_{22}$ - Mn_3Ga is -7.2%, -4.0%, -0.3% and 2.2% in respect to MgO, Cr, Pt and GaAs buffers, respectively. Therefore, it seems difficult to directly prepare smooth Mn_xGa films on MgO or sharp Mn_xGa -MgO interface for high-TMR MTJ due to the large misfit.^[50-53] Recently, Glas *et al.* also reported smooth Mn_xGa ($x=2.9$) films with root mean square (RMS) even below 0.25 nm on SrTiO₃.^[54] Zhu *et al.* reported Mn_xGa samples ($0.76 \leq x \leq 2.60$) grown on GaAs with good homogeneity and abrupt interfaces^[16,17] as revealed by the low-magnification TEM image in the inset of Fig. 2(a).

The structural and magnetic properties of Mn_xGa films could be tailored effectively by several reliable methods, such as by controlling growth temperature (T_s),^[16] tuning composition (x),^[17, 36] changing annealing conditions^[17] and selecting different substrates.^[42,43] In the following paragraphs, we will show in detail how T_s and x influence the structure and magnetism, taking Mn_xGa films grown on GaAs (001) as examples.

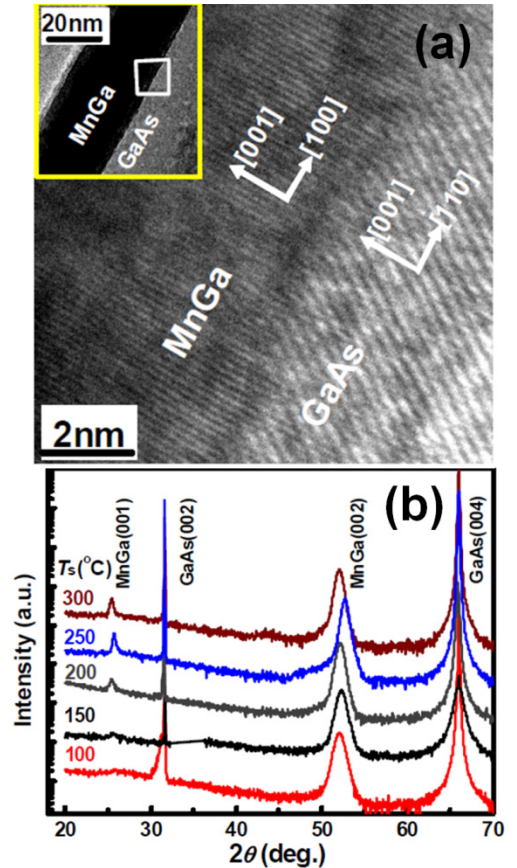


Fig. 2. (a) TEM image of MnGa films ($x=1.5$) grown on GaAs (001). The inset shows low-magnification TEM image. (b) XRD patterns of MnGa films ($x=1.5$) grown at 100, 150, 200, 250 and 300 °C, respectively. Reprinted with permission from [16].

Figure 2(a) shows representatively a high-resolution cross-sectional transmission electron microscopy (TEM) image of Mn_xGa films grown on GaAs,^[16] indicating a well-textured Mn_xGa layer with c -axis perpendicular to GaAs substrate. The epitaxial relationship of $MnGa(001)[100]||GaAs(001)[110]$ can be derived from the high-resolution TEM image, coinciding

with reflection high energy electron diffraction (RHEED) patterns. Figure 2(b) shows examples of synchrotron x-ray diffraction θ - 2θ patterns of Mn_xGa ($x=1.5$) films grown at different temperature.^[16] For all the films grown at temperatures from 100 to 350 °C, only sharp (001) superlattice peaks and (002) fundamental peaks of $L1_0$ - Mn_xGa films can be observed in the range from 20° to 70° besides the peaks of GaAs substrates, indicating that these are all (001)-textured single-crystalline films with c -axis along the normal direction, in agreement with cross-sectional TEM images and *in situ* RHEED patterns.

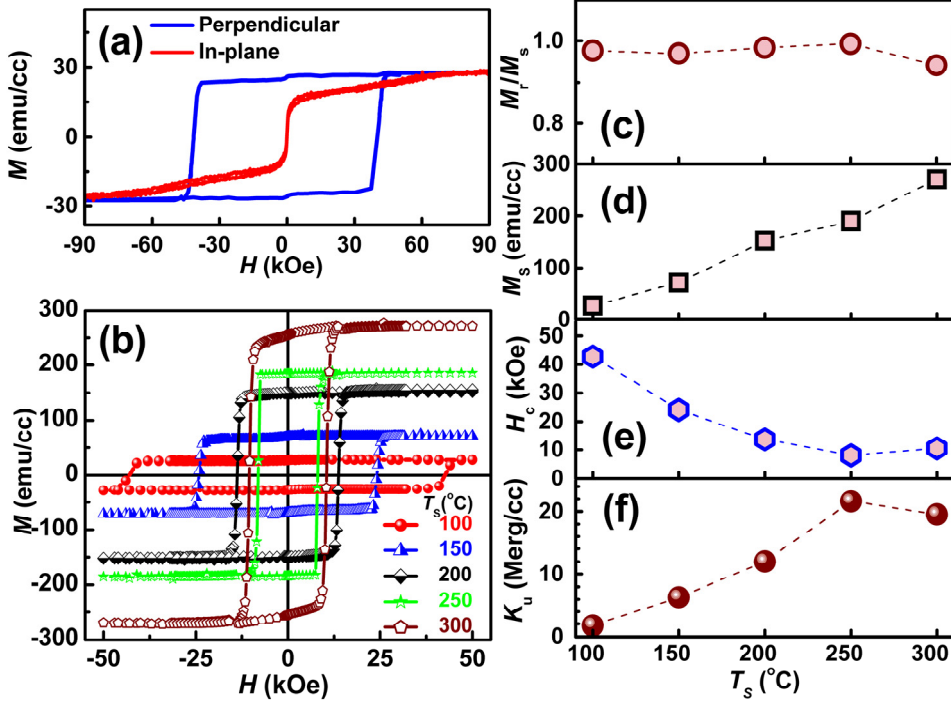


Fig.3. (a) Perpendicular and in-plane hysteresis loops of the 100 °C-grown $L1_0$ - $Mn_{1.5}Ga$ films measured by PPMS. (b) Perpendicular hysteresis loops of the $L1_0$ - $Mn_{1.5}Ga$ films grown at different temperature (T_s) measured by SQUID. (c) M_r/M_s , (d) M_s , (e) H_c and (f) K_u plotted as a function of T_s . Reprinted with permission from [16].

Figure 3(a) shows both perpendicular and in-plane hysteresis loops of a typical $Mn_{1.5}Ga$ film measured at 300 K.^[16] A nearly square loop with ultrahigh coercivity (H_c) of 42.8 kOe and remnant magnetization (M_r) of 27.3 emu/cc is observed from the perpendicular $M-H$ curve. However, the in-plane $M-H$ curve exhibits almost anhysteretic loop, zero remnant magnetization and high saturation field exceeding 90 kOe. This observation offers a direct evidence for the giant perpendicular magnetic anisotropy. The same feature holds for all the films grown at temperatures between 100 and 300 °C. Figure 3(b) shows the perpendicular $M-H$ curves of $Mn_{1.5}Ga$ films grown at different temperature, revealing a significant influence of growth temperature (T_s) on the magnetic properties. Figures 3(c)-3(f) summarize the values of M_r/M_s , M_s , H_c and K_u as a function of T_s . As shown in Fig. 3(c), M_r/M_s keeps a nearly invariant value large than 0.94 for all the films, very different from those of $L1_0$ - $Mn_{1.5}Ga$ films grown on GaN, GaSb, Si and Al_2O_3 .^[40-49] M_s increases monotonically from 27.3 to 270.5 emu/cc as T_s increases, which is much smaller than the calculated value of $2.51 \mu_B/Mn$ (~ 845 emu/cc) for stoichiometric $L1_0$ - $MnGa$ ^[16,21-23] due to both the

overall strains and off-stoichiometry. As shown in Fig. 3(e), H_c has a maximum of 42.8 kOe at 100 °C, then drops to 8.1 kOe at 250 °C, and finally climbs up to 10.8 kOe at 300 °C. The ultrahigh H_c in these $L1_0$ - $Mn_{1.5}Ga$ films was attributed to the combination of giant perpendicular magnetic anisotropy and imperfection including chemical disorder, lattice defects and overall tensile strains.^[16] Importantly, the imperfection contribution to H_c seems to be the same order of magnitude as the contribution from the magnetic anisotropy since H_c can be tailored so obviously over the large scale from 8.1 to 42.8 kOe. With increasing T_s , K_u goes up monotonically and reaches the maximum value at 250 °C and then decreases with further increasing T_s . The maximum K_u of 21.7 Merg/cc is roughly consistent with the theoretical value of 26 Merg/cc for $L1_0$ - $Mn_{50}Ga_{50}$,^[21] while much larger than reported Mn_xGa films grown on other semiconductors^[38-41] and MgO .^[22] Importantly, such a giant K_u of 21.7 Merg/cc in these $L1_0$ - $Mn_{1.5}Ga$ films supports nanoscale spintronic devices, such as spin-transfer-torque MRAMs bits, down to 5 nm in size and high-density bit-patterned recording with areal density up to 27 Tb/inch² and 60-year thermal stability.^[16]

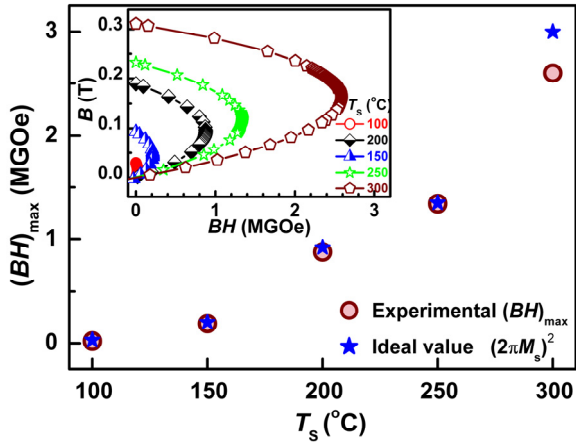


Fig. 4. Experimental magnetic energy products $(BH)_{\max}$ of $L1_0$ - $Mn_{1.5}$ Ga films with comparison with ideal value $(2\pi M_s)^2$. The inset shows the B - BH curves. Reprinted with permission from [16].

Magnetic materials with large magnetic energy product and noble-metal-free composition are also promising in permanent magnets applications.^[20] The magnetic energy product $(BH)_{\max}$ of $L1_0$ - Mn_x Ga films was further evaluated and compared with the ideal value $(2\pi M_s)^2$ in Fig. 4. $(BH)_{\max}$ climbs up monotonically from 0.02 to 2.60 MGOe as T_s increases and almost the same as ideal value $(2\pi M_s)^2$ when $T_s < 250$ °C because of the very high M_r/M_s . $(BH)_{\max}$ at $T_s = 300$ °C is slightly smaller than the ideal value probably due to the rounding at corner of M - H loops and the small difference between M_s and M_r ($M_r/M_s = 0.94$). The largest magnetic energy product up to 2.60 MGOe are observed in the film grown at 300 °C, which is larger than that previously reported in bulk polycrystalline DO_{22} - Mn_{2-3} Ga alloys (< 5.5 kJ/m³ or 0.68 MGOe)^[35] and steels magnets (~ 1 MGOe)^[20], and also comparable with hard ferrite magnets (~ 3 MGOe).^[20] Therefore, the rare-earth-free compositions, high coercivity and large magnetic energy product together make this kind of $L1_0$ - Mn_x Ga films promising to be developed for economical permanent magnets.

Both the structural and magnetic properties of Mn_x Ga epitaxial films were observed to be very sensitive to the composition. Recently, Mizukami *et al.* and Zhu *et al.* carried out symmetrical studies on the synthesis and strongly x -dependent magnetic properties of (001)-orientated Mn_x Ga epitaxial films with $x=1.2-3$ grown on Cr-buffered MgO (001)^[36] and films with $x=0.76-2.6$ grown on GaAs (001),^[17] respectively. Figure 5(a) shows examples of XRD θ - 2θ patterns of 250 °C-grown Mn_x Ga films with different x grown on GaAs (001) by MBE.^[17] For $0.76 \leq x \leq 1.75$, $L1_0$ - Mn_x Ga films shows both sharp (001) superlattice peaks and (002) fundamental peaks in the range from 20° to 70° besides the peaks of GaAs substrates, indicating that these are all (001)-textured single-crystalline films. For film with $x=0.74$, three small peaks irrelative to $L1_0$ appear,

which become dominating for film with $x = 0.55$. The new phase could be best fitted by cubic $MnGa_4$ with enlarged c axis of 3.91 Å. For film with $x = 2.60$, only the fundamental peak could be found due to the high disorder. As shown in Fig. 5(b), the x-ray reflection (XRR) curves with the strong oscillations suggest sharp interfaces and good homogeneity of these samples.

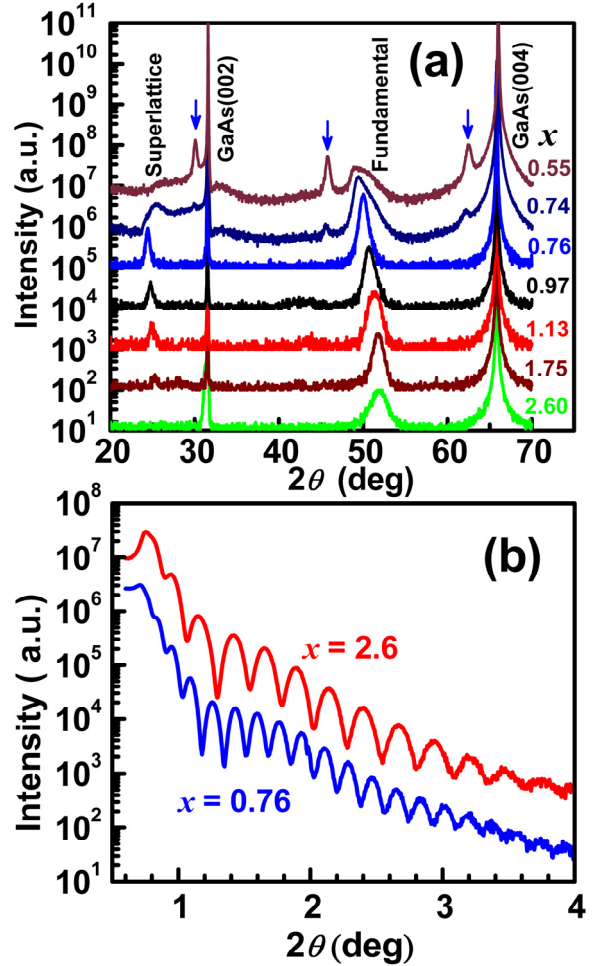


Fig. 5. (a) XRD patterns of MnGa films with different composition (x). (b) XRR curves of MnGa films with $x = 0.76$ and 2.6. Reprinted with permission from [17].

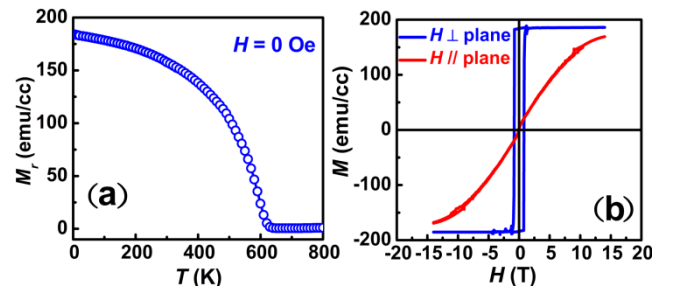


Fig. 6. (a) Temperature dependence of remanent magnetization (M_r); (b) Perpendicular and in-plane hysteresis loops of $Mn_{1.4}$ Ga films grown at 250 °C. Reprinted with permission from [17].

Figure 6(a) shows a typical temperature dependence of remanent magnetization of Mn_xGa films with Curie temperature of 630 K.^[17] Figure 6(b) show an example of hysteresis loops of $L1_0$ - $Mn_{1.4}Ga$ films grown at 250 °C.^[17] The sample exhibits a fairly square perpendicular loop with high perpendicular coercivity of 11 kOe and anhysteretic in-plane loops with giant saturation fields exceeding 14 T. These characteristics imply strong anisotropy existing in this kind of films.

Figures 7(a)-(c) display the x -dependent magnetic properties including M_r/M_s , M_s and H_c determined from the 300 K perpendicular M - H curves of these 250 °C-grown films. The Mn_xGa films with $x=0.97$ -1.75 exhibit high M_r/M_s exceeding 0.90; but those with x deviated from this range show dramatically decreased M_r/M_s . As shown in Fig. 7(b), M_s decreases dramatically from 450 to 52 emu/cc with x increases from 0.76 to 2.60, which should be attributed partly to the increase of antiferromagnetic coupling between Mn atoms at different sites,^[21] partly to the increase of strains induced by short c axis.^[16,23] The maximum M_s of 445 emu/cc in $Mn_{0.76}Ga$, is still below the calculated value of 845 emu/cc for stoichiometric $L1_0$ - $MnGa$ ^[16,21] and experimental value of 600 emu/cc in 400-450 °C-annealed $Mn_{1.17}Ga$ grown on MgO^[36] probably due to the low growth temperature. H_c climbs up from 4.38 to 20.1 kOe as x increases from 0.76 to 1.75, and then drops to 1.1 kOe at $x=2.60$. This change tendency is consistent well with that of K_u estimated in Fig. 7(d) following the method used in ref. 16. K_u exhibits large values from 8.6 to 21.0 Merg/cc in $L1_0$ range, while quickly degrades to 0.02 Merg/cc in $D0_{22}$ - $Mn_{2.6}Ga$ grown on GaAs because of increased disorder. Noticeably, $D0_{22}$ - Mn_xGa with high ordering and high quality may also demonstrate high K_u values, such as those grown on MgO substrates at high temperatures.^[36,45] As ever discussed,^[16,25] rare-earth-free and noble-metal-free Mn_xGa alloys are considerable for economical permanent magnet application. Since intrinsic coercivity H_c determined from M - H curves, normal coercivity H_{cB} determined from B - H curves and magnetic energy products $(BH)_{max}$ are three key features of quality of permanent magnets, we further calculated H_{cB} and $(BH)_{max}$ in Figs. 7(e) and (f). With increasing x in the phase-pure range, both H_{cB} and $(BH)_{max}$ decrease nearly monotonically, corresponding to the decrease of M_s . The film with $x = 1.07$ shows the highest H_{cB} and $(BH)_{max}$ of 3.6 kOe and 3.4 MGOe, respectively. The maximum of 3.4 MGOe is larger than that recent reported in $Mn_{1.5}Ga$ film (2.6 MGOe)^[16] and ferrite magnets (3 MGOe),^[20] which makes $L1_0$ - Mn_xGa alloys with low Mn compositions still promising to be developed for

cost-effective and high-performance permanent magnets applications. Taking into consideration of all the magnetic properties shown in Figs. 7(a)-7(f), low-Mn-composition $L1_0$ - Mn_xGa films are more advantageous than those $D0_{22}$ films to be developed for applications in magnetic recording with areal density over 10 Tb/inch², high-performance nanoscale spintronic devices like MRAM bits with size down to several nm and economical permanent magnet applications, since they simultaneously exhibit high M_r/M_s , M_s , K_u , H_c , H_{cB} and $(BH)_{max}$.

For further understanding of the composition-dependent magnetism, the structural and magnetic data for typical Mn_xGa films grown on MgO (001) substrates are summarized in Table 2. The magnetization of these films grown on MgO substrates degrades monotonically with increasing x , in consistence with on the case of Mn_xGa films grown on GaAs, which should be attributed partly to the increase of antiferromagnetic coupling between Mn atoms at different sites,^[21] partly to the increase of strains induced by short c axis.^[16,23] These films also demonstrated giant perpendicular anisotropy K_u of 10^6 - 10^7 erg/cc and huge coercivity H_c varying from 1 to 18 kOe. Noticeably, the values of H_c always tend to be larger in films with higher Mn-composition than films with lower Mn-composition, while values of K_u seem to have complicated dependences on compositions, probably due to the influence of different growth conditions or buffers.

It is also worth mentioning that the magnetism could be effectively tailored by post-growth annealing^[17] and choosing different substrates. By using different substrates like semiconductors (GaAs, GaSb, GaN, Si, ScN, etc), insulators (SiO₂, Al₂O₃, MgO, etc) and metals (Cr, Pt, etc), Mn_xGa films would crystallized into different structures, such as different crystalline orientation,^[42,43] different morphology^[35,47-49] and different strains,^[16] and further have different magnetic anisotropy and other magnetic properties.

Therefore, Mn_xGa films are observed to exhibit giant perpendicular magnetic anisotropy, flexible magnetization, huge coercivity, large energy products and high Curie temperature. Meanwhile, the magnetism of Mn_xGa films could be effectively tailored via several reliable ways, especially by controlling growth temperature, tuning compositions, post-growth annealing and selecting substrates. These data provide a comprehensive diagram for tailoring and improving the structure and magnetism of Mn_xGa films, which would be helpful for understanding this kind of material and approaching successful applications in a variety of spintronic devices, magnetic recording and permanent magnets

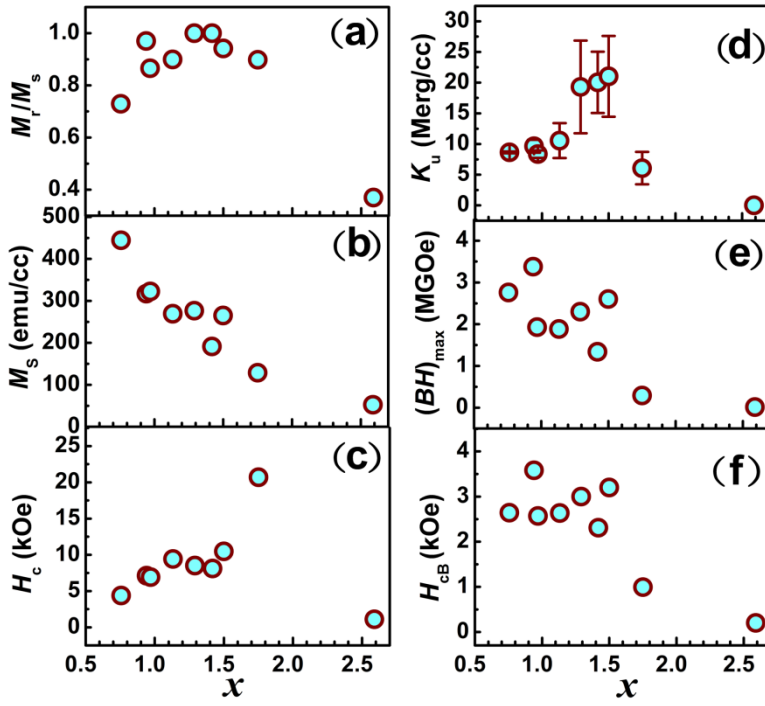


Fig. 7. Composition x dependence of (a) M_r/M_s , (b) M_s , (c) H_c and (d) K_u of Mn_xGa films grown on GaAs (001) at 250 °C. Reprinted with permission from [17].

Table 2 Structural parameters and magnetic data of typical Mn_xGa films grown on MgO (001). T represents growth or annealing temperature.

		T (°C)	a (Å)	c (Å)	M_s (300 K) (emu/cc)	K_u (300 K) (Merg/cc)	H_c (300 K) (kOe)	Reference
Mn_3Ga	Pt-MgO	250	-	7.12	110	8.9	18	[35, 47]
Mn_3Ga	MgO	350	-	7.07	140	19.1	18	[35, 47]
Mn_3Ga	Cr-MgO	350	-	6.96	140	4	17	[35, 47]
Mn_3Ga	Cr-MgO	400	-	7.10	200	-	15	[36]
$Mn_{2.5}Ga$	Cr-MgO	400	3.91	7.11	250	12	6	[46]
$Mn_{2.1}Ga$	MgO	450-500	3.92	7.11	305	15	-	[22]
Mn_2Ga	MgO	360	-	7.16	470	23.5	3.6	[35]
$Mn_{1.2}Ga$	Cr-MgO	400-500	3.90	3.60	600	15	1	[36]

2.3 Other spin-dependent properties of Mn_xGa epitaxial films

2.3.1 Spin polarization

For magnetic sensors, memories and oscillators, it is advantageous to use materials with high spin polarization, which allows for high magnetoresistance ratio and high signal to noise ratio. As calculated by Sakuma and Winterlik *et al.* stoichiometric $L1_0$ -MnGa and $D0_{22}$ - Mn_3Ga should have high spin polarization of 71% and 88% at the Fermi level, respectively.^[21,25] The spin polarization was also predicted to decrease with Mn deficiency, atomic disorder and strain.^[25] Kurt *et al.* performed point contact Andreev reflection spectroscopy measurements and determined spin polarization of 58% and 40% at 2.2 K in $D0_{22}$ - Mn_3Ga and Mn_2Ga films, respectively.^[47] Higher spin polarization was expected in perfectly ordered $D0_{22}$ - Mn_xGa films although detailed investigations are still missing. To our best knowledge, there have also been no

available reports about experimental measurements of spin polarization of $L1_0$ - Mn_xGa alloys. Further investigations on spin polarization are needed.

2.3.2 Magnetic damping

Spin-transfer-torque (STT) is a phenomenon of magnetization switching induced by spin current. For STT-driven spintronic devices, a low critical current for current-induced magnetization switching is preferred for low energy consumption and reliable switching.^[2,55] The critical switching current can be written as:

$$I_{C0} = \alpha K_u V \frac{\gamma e}{\mu_B g(P, \theta)} \quad (1)$$

where α is magnetic damping constant; K_u , perpendicular anisotropy; V , volume of magnets; γ , gyromagnetic ratio; μ_B , Bohr magneton; e , the elementary charge; $g(P, \theta)$, function of spin

polarization (P) of tunnel current and the angle (θ) between the magnetization of the free and the reference layers.

As indicated in Eq. (1), perpendicular magnetized materials with combination of high P , low α and low K_u are preferred for low-switching-current STT device applications. Generally, a high K_u and a low critical switching current I_{c0} are in contrast, but high K_u is absolutely essential for long time stability. However, a combination of high P and K_u with low enough α could still provide a possibility for a low I_{c0} and long time thermal stability. Except for the high P and K_u , the noble-metal-free Mn_xGa alloys also have much lower magnetic damping constants than those of all the other perpendicular-anisotropy materials to our best knowledge, due to the low density of states at the Fermi level and the weak spin-orbit interaction in light $3d$ elements Mn and Ga.^[22] Time-resolved MOKE experiment revealed the damping constants of 0.008 (0.015) for $Mn_{1.54}Ga$ ($Mn_{2.12}Ga$) films, which are one or two order smaller than that of known materials with large perpendicular anisotropy.^[2] First-principles calculations indicate even lower damping constant of 0.0003 (0.001) for $L1_0$ - $MnGa$ ($D0_{22}$ - Mn_3Ga) defect-free alloys.^[22] Therefore, with respect to both high thermal stability and low critical switching current, Mn_xGa alloys with either $L1_0$ or $D0_{22}$ ordering are advantageous for low-current-switching STT-memory and oscillator applications.

2.3.3 Magneto-optical Kerr effect

Perpendicularly magnetized materials with large Kerr rotation angle and optical reflectivity are also promising in high-density perpendicular magneto-optical recording. Krishnan first studied the magneto-optical properties of $L1_0$ - $Mn_{1.5}Ga$ films grown on GaAs (001) in 1992.^[38] The film exhibited a large Kerr rotation angle of $\sim 0.1^\circ$ at 820 nm. Furthermore, reflectivity around 65%-70% were found over a broad wavelength range from ultraviolet to far infrared. From a technological point of view, the epitaxial growth on semiconductor and the high-performance magneto-optical properties would make the exciting possibility of the integration of magneto-optic and semiconductor devices a reality.

2.3.4 Anomalous Hall effect

Anomalous Hall effect (AHE), related to spin-orbit interaction in magnetic materials, has potential for sensor, memory and magnetic logic applications.^[45] Large AHE has been observed in various PMA films including $L1_0$ -FePt, FePd, etc.^[56,57] Accordingly, study of AHE in Mn_xGa films is of great importance not only for practical applications but also helpful for comprehending the widely disputed mechanism of AHE. Tanaka *et al.*

measured the AHE hysteresis of $L1_0$ - $Mn_{1.5}Ga$ films on GaAs and found the AHE resistivity sample-dependent, changing from 0.5-4 $\mu\Omega\cdot\text{cm}$.^[39] Bedoya-Pinto revealed noticeably composition-dependent scaling behavior in $L1_0$ - Mn_xGa ($x=0.96, 1.38$ and 2.03) films on GaN.^[41] Wu *et al.* observed AHE resistivity up to 11.5 $\mu\Omega\cdot\text{cm}$ in $D0_{22}$ - Mn_2Ga ,^[45] which is much larger than that of other perpendicular-anisotropy materials, such as $L1_0$ -FePt (1-6 $\mu\Omega\cdot\text{cm}$).^[56,57] Glas *et al.* studied $D0_{22}$ - Mn_xGa ($x=2.3, 2.6$ and 2.9) films grown on MgO and SrTiO₃, and discussed the determined skew scattering and side jump coefficients with regard to the film composition and compared to the crystallographic and magnetic properties.^[54] Zhu *et al.* reported AHE and the scaling behavior of $L1_0$ - $Mn_{1.5}Ga$ films grown on GaAs (001) and found significant influence of disorder on the scaling behaviors.^[58] However, for further understanding of the underlying physics, more detailed studies will be needed.

2.4. Thermal and Chemical stability

Structural stability of materials is of particular importance for practical applications. $L1_0$ -ordered Mn_xGa have been widely believed to keep thermal-dynamically stable up to at least 800 K,^[31,32] by contrast, Mn_xGa with $D0_{22}$ -ordering are observed to be metastable and will transfer to antiferromagnetic hexagonal $D0_{19}$ phase at temperature over 770 K.^[25,33,34] Zhu *et al.* investigated the thermal stability of MnGa/GaAs interface by performing systematical post-growth annealing experiments taking $L1_0$ - $Mn_{0.76}Ga$ film as an example, which exhibits the largest M_s among all the as-grown films with different x (Fig. 7(b)). Figure 8(a) shows XRD patterns of as-grown and 10 min-annealed $Mn_{0.76}Ga$ films, from which we found the $Mn_{0.76}Ga$ film itself is thermal stable up to 450 $^\circ\text{C}$, and the interface could keep stable up to at least 350 $^\circ\text{C}$. This result roughly agrees with previous report that Mn_xGa with $x < 1.5$ should keep stable on GaAs below 400 $^\circ\text{C}$.^[59] Interestingly, very weak Mn_2As (003) peak as a result of interfacial reaction is observable by high-sensitivity synchrotron XRD measurement, which may be undetectable by common XRD with Cu $K\alpha$ radiation.^[59] Fortunately, the stable temperature of at least 350 $^\circ\text{C}$ could still satisfy the demand of integration with metal-oxide-semiconductor transistors.

As to the chemical stability in the ambient conditions, there have been disputations on the chemical stability of Mn_xGa alloys. Roy *et al.* found an oxide layer of less than 5 nm formed at the Mn_xGa surface,^[60] but Wang *et al.* found no signs of oxidation of Mn_xGa films in air atmosphere.^[61] In fact, a capping layer is always used to prevent possible oxidation of Mn_xGa film.^[16,36,38] In order to make clear the chemical stability in the ambient

conditions, we show in Fig. 8(b) x-ray photoelectron spectroscopy (XPS) of Mn and Ga on the surfaces of Mn_xGa films with and without capping layer which were exposed in the air at room temperature for a week.^[24] Mn_xGa films with Al capping layer showed asymmetric elemental peaks for both Mn 2*p* and Ga 3*d* spectrums. The asymmetry of these peaks should be attributed to the significant shielding effect to the core levels by the high-density at the Fermi level due to the alloy nature of the film, which further reveals the good protection of a 2 nm Al layer from oxidation. By contrast, Mn_xGa films without Al capping layer showed evident peak shifts and reduced asymmetry, indicating significant oxidation occurred. Therefore, it is necessary to protect Mn_xGa films from oxidation by using suitable capping layers.

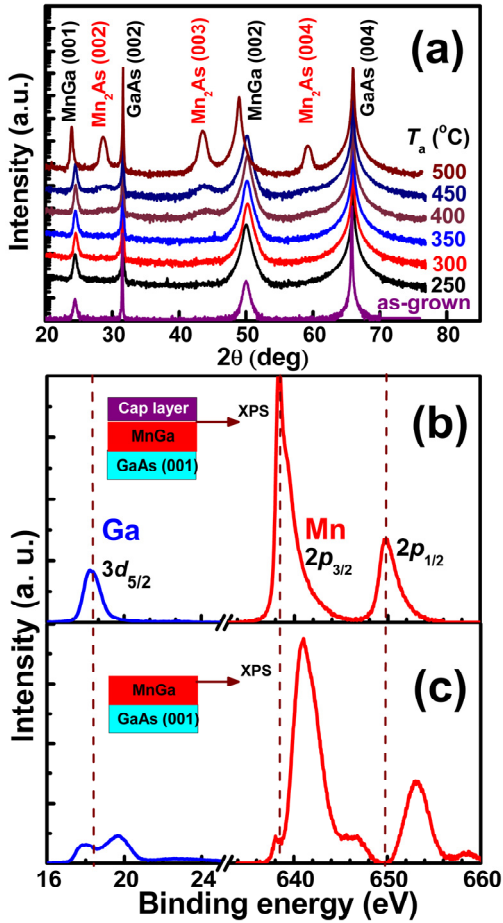


Fig. 8 (a) XRD patterns of $Mn_{0.76}Ga$ films annealed at 250, 300, 350, 400, 450 °C, respectively (Reprinted with permission from [17]); XPS patterns of $Mn_{0.97}Ga$ films (b) with and (c) without Al cap layer after exposed in air atmosphere for a week (Reprinted with permission from [24]).

2.5. Mn_xGa -based spintronic devices

Magnetic tunneling junctions (MTJ) and giant magnetoresistance (GMR) devices based on perpendicularly magnetized materials are expected to ensure thermal stability of nanoscale spintronic devices and to be developed as high-performance

MR sensors, STT-MRAM and STT-oscillators. As discussed above, (001)-orientated Mn_xGa alloys with $L1_0$ or DO_{22} ordering simultaneously show giant K_u , high P , high T_c , huge H_c , moderate M_s and low α , which make this kind of material an ideal combination for high-field sensors, Gbit STT-MRAM and high-power STT-oscillators. Recently, a few groups have carried out theoretical and experimental work from this point of view. Using first-principle calculations based on density functional theory and non-equilibrium Green's function, Bai *et al.* predicted large tunnel magnetoresistance (TMR) effect of 1000% in $Mn_2Ga/MgO/Mn_2Ga$ magnetic tunnel junctions, whereas no tunneling magnetoresistance effect in the $Mn_3Ga/MgO/Mn_3Ga$ MTJ stack due to the symmetry selective spin filtering effect of MgO.^[62] Kubota *et al.* observed TMR ratios no more than 23% at 10 K and annealing endurance up to 375 °C in a series of $Mn_xGa/MgO/CoFe$ MTJ with different compositions of Mn_xGa electrode.^[50] The small TMR ratios were attributed to the large misfit between MgO and Mn_xGa , which may cause lattice dislocations and an unfavorable growth of the MgO barrier. Kubota *et al.* further made attempts to improve TMR ratios by using Fe or Mg insertion layers between Mn_xGa and MgO interface,^[51,52] however, the optimized TMR ratios still below 25% at 10 K. So far, the highest TMR ratio in Mn_xGa -based MTJs is 40% at room temperature observed in $Mn_{1.63}Ga/MgO/CoFeB$ MTJ with Co (1.5 nm)/Mg (0.4 nm) insertion between $Mn_{1.63}Ga$ and MgO.^[53] Noticeably, Zha *et al.* also fabricated (112)-textured $Mn_{2.3-2.4}Ga/Cu/CoFe$ current-in-plane pseudo spin valve with GMR up to 3.88%.^[63] Roy *et al.* studied the oscillatory dependence of the interlayer exchange coupling strength on spacer layer thickness in $Mn_xGa/GaAs$ (Mn_2As , Mn_2Sb)/ Mn_xGa trilayers.^[64] In addition, Adelman *et al.* demonstrated electrical spin-injection from $Mn_{1.38}Ga$ into (Al,Ga)As *p-i-n* light-emitting diode (LED) at remanence.^[12]

It is still an open issue to explore Mn_xGa -based MTJ, spin valve devices and semiconductor spintronic devices with high performance for practical applications, and take advantage of the amazing properties of this candidate material.

3. $L1_0$ - Mn_xAl epitaxial films on semiconductors

3.1 Lattice structure and synthesis of Mn_xAl bulks

Despite the complex phase diagram (Fig. 9),^[65] alloys of Mn and Al only have one ferromagnetic phase with a lattice unit similar to that of $L1_0$ - $MnGa$ (i.e. τ -phase) shown in Fig. 1(b). The lattice constants of $L1_0$ - $MnAl$ bulk are $a=3.92$ Å and $c=3.57$ Å.^[66] In 1960, Koch *et al.* synthesized $L1_0$ - $Mn_{1.25}Al$ bulk by rapid cooling of nonmagnetic ϵ - $MnAl$ and observed T_c of 653 K, M_s of 490 emu/cc,

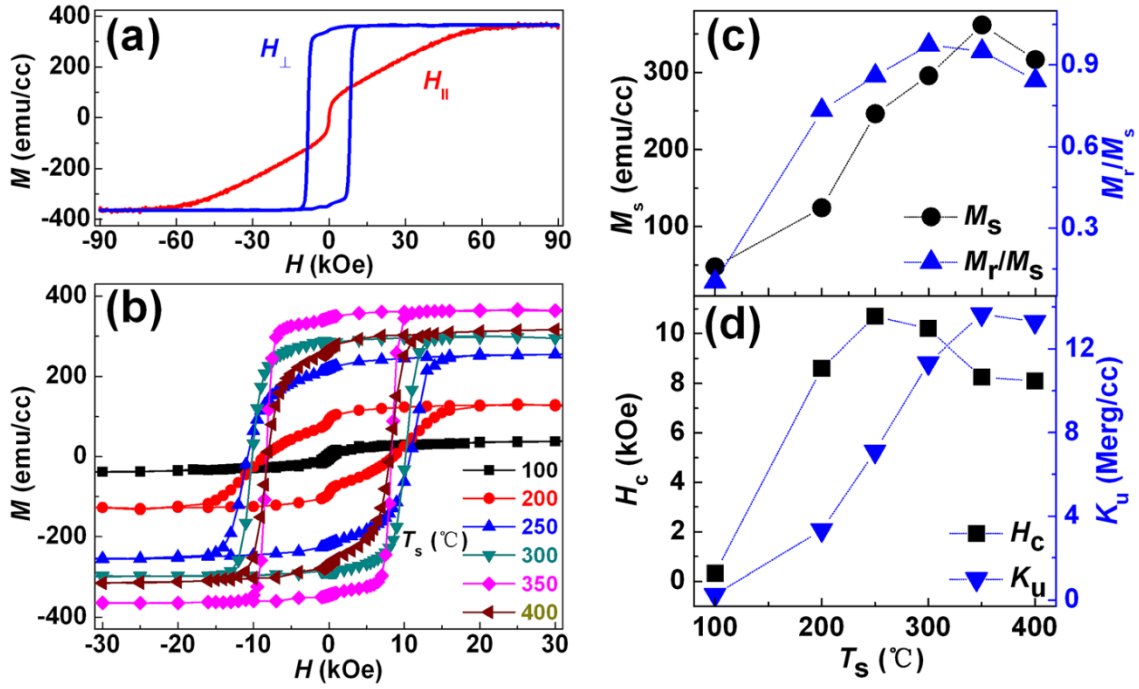


Fig. 11. (a) Perpendicular and in-plane hysteresis loops of the 350 °C-grown $L1_0$ - $Mn_{1.1}Al$ films. (b) Perpendicular hysteresis loops of the $L1_0$ - $Mn_{1.1}Al$ films grown at different temperature (T_s). (c) M_r/M_s , M_s , (d) H_c and K_u plotted as a function of T_s . Reprinted with permission from [26].

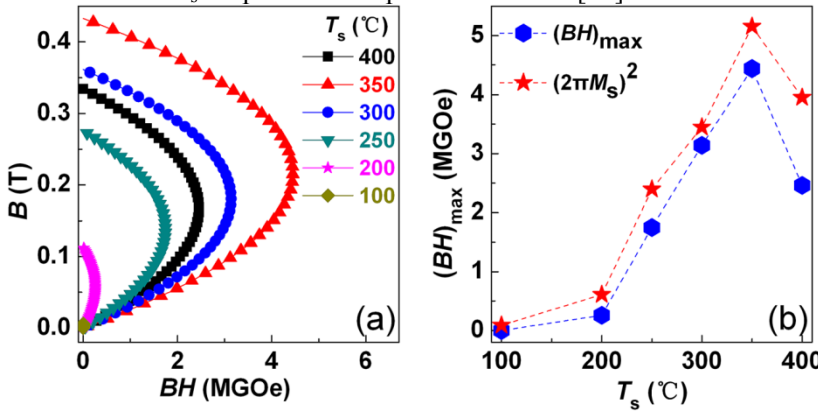


Fig. 12 (a) T_s dependence of the magnetic energy products. (b) Comparison of the experimental $(BH)_{max}$ with ideal value $(2\pi M_s)^2$. Reprinted with permission from [26].

For better understanding, the typical data of structure and magnetic properties of MnAl films grown on different buffers are compared in Table 3. Mn_xAl films grown on AlAs and GaAs buffers exhibited much lower magnetization than bulk and

films grown on Cr-MgO, which is probably related to the shorter c -axis and corresponding strains. Noticeably, despite the different buffers and growth (annealing) temperature, all these MnAl films display a high K_u exceeding 10 Merg/cc.

Table 3 Structure parameters and magnetic data for representative Mn_xAl films grown on different substrates. T_s (T_a) represents growth (annealing) temperature.

		T_s (T_a) (°C)	a (Å)	c (Å)	M_s (300 K) (emu/cc)	K_u (300 K) (Merg/cc)	H_c (300 K) (kOe)	Reference
Mn _{1.50} Al	AlAs-Ga As	200~270 (350)	-	3.41	285	-	~4.0	[73]
Mn _{1.11} Ga	GaAs	350	-	3.47	361	13.7	~8.0	[26]
Mn _{1.32} Al	Cr-MgO	250 (250)	-	~3.57	530	10	-	[75]
Mn _{0.92} Al	Cr-MgO	200 (450)	3.92	3.57	600	10	-	[76]

3.3 Other spin-dependent properties

3.3.1 Magneto-optical Kerr effect

Cheeks *et al.* investigated the polar magneto-optical Kerr effect in 5 and 10 nm thick $L1_0$ -MnAl epitaxial films grown on AlAs-buffered GaAs (001) and found a large Kerr rotation of 0.11° in a wide wave length range from 220 to 820 nm.^[71] The 0.11° value is modest compared to the 0.3 - 0.4° values reported for materials such as TbFeCo, currently used in the industry. Although thicker films are expected to give higher Kerr rotation, there is so far no further progress report available.

3.3.2 Anomalous Hall effect

The anomalous Hall effect of $L1_0$ -MnAl films were intensively studied in 1990s. Sands *et al.*^[68] and Leadbeater *et al.*^[69] prepared single-crystalline $L1_0$ -MnAl films on AlAs-GaAs (001) with a perpendicular c -axis and observed a large Hall hysteresis. Angadi and Thanigaimani reported the Hall effect of MnAl films evaporated on glass substrates with different compositions and thickness (25-150 nm), and found that the ordinary Hall coefficient R_0 and anomalous Hall coefficient R_s are of the same order over the entire thickness range.^[77] Both R_0 and R_s are positive for lower thickness, and negative for higher thickness. Boeck *et al.* observed rectangular Hall hysteresis loops in $Mn_{1.5}Al$ grown on AlAs-GaAs (001) and AHE resistivity in the order of 4 - $8 \mu\Omega\text{cm}$,^[72] depending on width of Hall bars. Despite of these progresses, detailed knowledge about the microscopic mechanism of AHE in this kind of material remains a shortage and needs further exploration in the future.

4. Conclusions and outlook

Numerous studies have been carried out on the synthesis and characterizations of Mn_xGa and Mn_xAl epitaxial films with perpendicular anisotropy. Mn_xGa alloys with both $L1_0$ and $D0_{22}$ ordering show giant perpendicular anisotropy, high spin polarization, high Curie temperature, huge coercivity, moderate magnetization, large energy product, low damping constant, giant Kerr rotation and large anomalous Hall resistivity and high thermal dynamical stability. $L1_0$ -ordered Mn_xAl films grown on GaAs and MgO also exhibit giant perpendicular anisotropy, high Curie temperature, huge coercivity, moderate magnetization, large energy product, giant Kerr rotation and large anomalous Hall resistivity (2 - $8 \mu\Omega\text{cm}$). Importantly, the magnetism of both Mn_xGa and Mn_xAl films could be tailored effectively by several methods including controlling growth temperature, tuning composition, varying annealing conditions and selecting different substrates. These pronounced magnetic properties and effective controllability make these perpendicularly magnetized Mn-based binary alloy films much promising for high-performance novel spintronic devices, ultrahigh-density perpendicular magnetic recording and economical permanent

magnets, although there have rarely been progress on high-performance spintronic devices, magnetic recording or practical permanent magnets applications. Moreover, the Mn_xGa and Mn_xAl ferromagnetic films with both high K_u and good compatibility with semiconductor have great applications in not only semiconductor spintronics like spin-LED, spin-FET, and lateral spin valves with perpendicular spin injectors and detectors, but also in high-density integration of metallic spintronics functional devices like nonvolatile magneto-resistive random access memory on semiconductor photonic and electronic circuits.

We expect more detailed exploration on fundamental issues as to detailed knowledge on spin polarization, magnetic damping and AHE of Mn_xGa and Mn_xAl alloys, and possible practical applications like ultrahigh-density magnetic recording, economical permanent magnets, nonvolatile memory, high-field magnetoresistive sensors and high-performance oscillators and semiconductor spintronic devices with perpendicular injectors and detectors taking advantage of the amazing properties of this candidate material. It is also admirable to explore new kinds of ferromagnetic films with both high K_u and good compatibility with semiconductors. We are also looking forward to new progress on high-density integration of metallic spintronics functional devices with semiconductor circuits taking advantage of such films.

References

- [1] Chappert C, Fert A and Dau F N V, 2007 *Nature Mater.* **6**, 813
- [2] Ikeda S, Miura K, Yamamoto H, Mizunuma K, Gan H D, Endo M, Kanai S, Hayakawa J, Matsukura F and Ohno H, 2010 *Nat. Mater.* **9**, 721
- [3] Mangin S, Ravelosona D, Katine J A, Carey M J, Terris B D and Fullerton E E, 2006 *Nat. Mater.* **5**, 210
- [4] Houssameddine D, Ebels U, Delaët B, Rodmacq B, Firastrau I, Ponthenier F, Brunet M, Thirion C, Michel J -P, Prejbeanu-Buda L, Cyrille M C, Redon O and Diény B, 2007 *Nat. Mater.* **6**, 447
- [5] Mancoff F B, Dunn J H, Clemens B M and White R L, 2000 *Appl. Phys. Lett.* **77**, 1879
- [6] Datta S and Das B, 1990, *Appl. Phys. Lett.* **56**, 665
- [7] Koo H C, Kwon J H, Eom J, Chang J, Han S H and Johnson M 2009 *Science* **325**, 1515
- [8] Wunderlich J, Park B, Irvine A C, Zárbo L P, Rozkotová E, Nemeč P, Novák V, Sinova J and Jungwirth T, 2010 *Science* **330**, 1801
- [9] Kohda M, Kita T, Ohno Y, Matsukura F and Ohno H, 2006 *Appl. Phys. Lett.* **89**, 012103
- [10] Ohno Y, Young D K, Beschoten B, Matsukura F, Ohno H and Awschalom D D, 1999, *Nature*, **402**, 790
- [11] Lou X, Adelman C, Crooker S A, Garlid E S,

- Zhang J J, Reddy K S M, Flexner S D, Palmström C J and Crowell P A, 2007 *Nat. Mater.* **3**, 197
- [12] Adelman C, Hilton J L, Schultz B D, McKernan S, Palmström C J, Lou X, Chiang H S and Crowell P A, 2006 *Appl. Phys. Lett.* **89**, 112511.
- [13] Lu E, Ingram D C, Smith A R, Knepper J W and Yang F Y, 2006 *Phys. Rev. Lett.* **97**, 146101.
- [14] Tanaka M, Harbison J P, DeBoeck J, Sands T, Philips B, Cheeks T L and Keramidias V G, 1993 *Appl. Phys. Lett.* **62**, 1565.
- [15] Krishnan K M, 1992 *Appl. Phys. Lett.* **61**, 2365
- [16] Zhu L J, Nie S H, Meng K K, Pan D, Zhao J H and Zheng H Z, 2012 *Adv. Mater.* **24**, 4547
- [17] Zhu L J, Pan D, Nie S H, Lu J and Zhao J H, 2013 *Appl. Phys. Lett.* **102**, 132403
- [18] Ohno H, 2010 *Nat. Mater.* **9**, 952
- [19] Challenger W A, Peng C, Itagi A V, Karns D, Peng W, Peng Y G, Yang X M, Zhu X B, Gokemeijer N J, Hsia Y T, Ju G, Rottmayer R E, Seigler M A and Gage E C, 2009 *Nat. Photon* **3**, 220
- [20] Gutfleisch O, Willard M A, Brück E, Chen C H, Sankar S G and Liu J P, 2011 *Adv. Mater.* **23**, 821
- [21] Sakuma A, 1998 *J. Magn. Magn. Mater.* **187**, 105
- [22] Mizukami S, Wu F, Sakuma A, Walowski J, Watanabe D, Kubota T, Zhang X, Naganuma H, Oogane M, Ando Y and Miyazaki T, 2011 *Phys. Rev. Lett.* **106**, 117201
- [23] Yang Z, Li J, Wang D, Zhang K and Xie X, *J. Magn. Magn. Mater.* **182**, 369
- [24] Zhu L J and Zhao J H, 2013 *Appl. Phys. A* **111**, 379
- [25] Winterlik J, Balke B, Fecher G H, Felser C, Alves M C M and Bernardi F, Morais J, 2008 *Phys. Rev. B* **77**, 054406
- [26] Nie S H, Zhu L J, Lu J, Pan D, Wang H L, Yu X Z, Xiao J X and Zhao J H 2013 *Appl. Phys. Lett* **102**, 152405
- [27] Sakuma A 1994 *J. Phys. Soc. Jpn.* **63**, 1422
- [28] Meissner HG and Schubert K, 1965 *Z. Metallkd.* **56**, 523
- [29] Wu J S and Kuo K H, 1997 *Metall. Mater. Trans. A* **28A**, 729
- [30] Massalski T B, 1990 *Binary Alloy Phase Diagrams*, 2nd edn. (Ohio: Materials Information Soc., Materials Park)
- [31] Bither T A and Cloud W H, 1965 *J. Appl. Phys.* **36**, 1501
- [32] Lu X, Liang J and Yang Z, 1979 *Acta Phys. Sin.* **28**, 54 (in Chinese)
- [33] Krén E and Kádár G, 1970 *Solid State Commun.* **8**, 1653
- [34] Niida H, Hori T, Onodera H, Yamaguchi Y and Nakagawa Y, 1996 *J. Appl. Phys.* **79**, 5946
- [35] Kurt H, Rode K, Venkatesan M, Stamenov P and Coey J M D, 2011 *Phys. Status. Solidi B* **248**, 2338
- [36] Mizukami S, Kubota T, Wu F, Zhang X, Miyazaki T, Naganuma H, Oogane M, Sakuma A and Ando Y, 2012 *Phys. Rev., B* **85**, 014416
- [37] Huh Y, Kharel P, Shah V R, Li X Z, Skomski R and Sellmyer D J, 2013 *J. Appl. Phys.* **114**, 013906
- [38] Krishnan K M, 1992 *Appl. Phys. Lett.* **61**, 2365
- [39] Tanaka M, Harbison J P, DeBoeck J, Sands T, Philips B, Cheeks T L and Keramidias V G, 1993 *Appl. Phys. Lett.* **62**, 1565
- [40] Lu E, Ingram D C, Smith A R, Knepper J W and Yang F Y, 2006 *Phys. Rev. Lett.* **97**, 146101
- [41] Bedoya-Pinto A, Zube C, Malindretos J, Urban A and Rizzi A, 2011 *Phys. Rev. B* **84**, 104424
- [42] Wang K, Lu E, Knepper J W, Yang F and Smith A R, 2011 *Appl. Phys. Lett.* **98**, 162507
- [43] W. Feng, D. V. Thiet, D. D. Dung, Y. Shin and S. Chob, 2010 *J. Appl. Phys.* **108**, 113903
- [44] Wang K, Chinchore A, Lin W, Ingram D C, Smith A R, Hauser A J and Yang F, 2009 *J. Cry. Growth* **311**, 2265
- [45] Wu F, Sajitha E P, Mizukami S, Watanabe D, Miyazaki T, Naganuma H, Oogane M and Ando Y, 2010 *Appl. Phys. Lett.* **96**, 042505
- [46] Wu F, Mizukami S, Watanabe D, Naganuma H, Oogane M and Ando Y, 2009 *Appl. Phys. Lett.* **94**, 122503
- [47] Kurt H, Rode K, Venkatesan M, Stamenov P and Coey J M D, 2011 *Phys. Rev. B* **83**, 020405(R)
- [48] Nummy T J, Bennett S P, Cardinal T and Heiman D, 2011 *Appl. Phys. Lett.* **99**, 252506
- [49] Zha C L, Dumas R K, Lau J W, Mohseni S M, Sani S R, Golosovsky I V, Monsen Å F, Nogués J and Åkerman J, 2011 *J. Appl. Phys.* **110**, 093902
- [50] Kubota T, Araidai M, Mizukami S, Zhang X, Ma Q, Naganuma H, Oogane M, Ando Y, Tsukada M and Miyazaki T, 2011 *Appl. Phys. Lett.* **99**, 192509
- [51] Kubota T, Mizukami S, Watanabe D, Wu F, Zhang X, Naganuma H, Oogane M, Ando Y and Miyazaki T, 2011 *J. Appl. Phys.* **110**, 013915
- [52] Kubota T, Ma Q, Mizukami S, Zhang X, Naganuma H, Oogane M, Ando Y and Miyazaki T, 2012 *Appl. Phys. Express* **5**, 043003
- [53] Ma Q L, Kubota T, Mizukami S, Zhang X M, Naganuma H, Oogane M, Ando Y and Miyazaki T, 2012 *Appl. Phys. Lett.* **101**, 032402
- [54] Glas M, Imort I–M, Thomas P, Reiss G and Ebke D, 2013 *J. Magn. Magn. Mater.* **333**, 134
- [55] Brataas A, Kent A D and Ohno H, 2012 *Nat. Mater.* **11**, 372
- [56] Yu J, Ruediger U, Kent A D, Farrow R F C, Marks R F, Weller D, Folks L and Parkin S S P, 2000 *J. Appl. Phys.* **87**, 6854
- [57] He P, Ma L, Shi Z, Guo G Y, Zheng J G, Xin Y and Zhou S M, 2012 *Phys. Rev. Lett.* **109**, 066402
- [58] Zhu L J, Pan D and Zhao J H, “Proper scaling of anomalous Hall effect in disordered $L1_0$ -Mn_{1.5}Ga”, (submitted)
- [59] Hilton J L, Schultz B D, McKernan S and Palmström C J, 2004 *Appl. Phys. Lett.* **84**, 3145

- [60] Roy W V, Akinaga H, Miyanishi S, Tanaka K and Kuo L H, 1996 *Appl. Phys. Lett.* **69**, 711
- [61] K. Wang, A. Chinchore, W. Lin, A. Smith and K. Sun, 2009 *MRS. Proceedings*, 1118, 1118-K06-06
- [62] Z. Bai, Y. Cai, L. Shen, M. Yang, V. Ko, G. Han and Y. Feng, 2012 *Appl. Phys. Lett.* **100**, 022408
- [63] C. L. Zha, R. K. Dumas, J. Persson, S. M. Mohseni, J. Nogués and J. Åkerman, 2010 *IEEE Mag. Lett.* **1**, 2500104
- [64] W. V. Roy, H. Akinaga and S. Miyanishi, 2001 *Phys. Rev. B* **63**, 184417
- [65] Jiménez-Villacorta F, Marion J L, Sepehrifar T, Daniil M, Willard M A and Lewis L H, 2012 *Appl. Phys. Lett* **100**, 112408
- [66] Koch A J J, Hokkeling P, Steeg M G and Vos K J 1960 *J. Appl. Phys.* **31**, 75S
- [67] Ohtani T, Kato N, Kojima K, Sakamoto Y, Konno I, Tsukahara M and Kubo T, 1997, *IEEE Trans. Magn.* **13**,5
- [68] Sands T, Harbison J P, Leadbeater M L, Allen S J, Hull G W, Ramesh R, Florez L T and Keramidas V. G 1990 *Appl. Phys. Lett* **57**, 2609
- [69] Leadbeater M L, Allen S J, DeRosa F, Harbison J P, Sands T, Ramesh R, Florez L T and Keramidas V. G 1991 *J. Appl. Phys.* **69**, 4689
- [70] Nie S H, Zhu L J, Pan D, Lu J and Zhao J H 2013 *Acta Phys. Sin.* (in Chinese) (to be published)
- [71] Cheeks T L, Brasil M J S P, Sands T, Harbison J P, Aspnes D E, Keramidas V G and Allen S J, 1992 *Appl. Phys. Lett* **60**, 1393
- [72] Boeck J D, Sands T, Harbison J P, Scherer A, Gilchrist H, Cheeks T L, Tanaka M and Keramidas V G, 1993 *Electronics Lett.* **29**, 421
- [73] Roy W V, Boeck J D, Bender H, Bruynseraede C, Esch A V and Borghs G, 1995, *J. Appl. Phys.* **78**, 398
- [74] Rosier T M, He Y W and El-Masry N A, 1996 *Mater. Lett.* **26**, 227
- [75] Saruyama H, Oogane M, Kurimoto Y, Naganuma H and Ando Y, 2013 *Jpn. J. Appl. Phys.* **52**, 063003
- [76] Hosoda M, Oogane M, Kubota M, Kubota T, Saruyama H, Lihama S, Naganuma H and Ando Y, 2012, *J. Appl. Phys.* **111**, 07A324
- [77] Angadi M A and Thanigaimani V, 1991, *Thin Solid Films*, **195**,7